

GLADMamba: Unsupervised Graph-Level Anomaly Detection Powered by Selective State Space Model

Yali Fu¹, Jindong Li², Qi Wang^{1,3} (✉), and Qianli Xing¹

¹ Jilin University, Changchun, China

fuy123@mails.jlu.edu.cn, {qiwang,qianlixing}@jlu.edu.cn

² Hong Kong University of Science and Technology (Guangzhou), Guangzhou, China

jli839@connect.hkust-gz.edu.cn

³ Engineering Research Center of Knowledge-Driven Human-Machine Intelligence, Ministry of Education, China

Abstract. Unsupervised graph-level anomaly detection (UGLAD) is a critical and challenging task across various domains, such as social network analysis, anti-cancer drug discovery, and toxic molecule identification. However, existing methods often struggle to capture the long-range dependencies efficiently and neglect the spectral information. Recently, selective State Space Models (SSMs), particularly Mamba, have demonstrated remarkable advantages in capturing long-range dependencies with linear complexity and a selection mechanism. Motivated by their success across various domains, we propose GLADMamba, a novel framework that adapts the selective state space model into UGLAD field. We design View-Fused Mamba (VFM) with a Mamba-Transformer-style architecture to efficiently fuse information from different views with a selective state mechanism. We also design Spectrum-Guided Mamba (SGM) with a Mamba-Transformer-style architecture to leverage the Rayleigh quotient to guide the embedding refining process. GLADMamba can dynamically focus on anomaly-related information while discarding irrelevant information for anomaly detection. To the best of our knowledge, this is the first work to introduce Mamba and explicit spectral information to UGLAD. Extensive experiments on 12 real-world datasets demonstrate that GLADMamba outperforms existing state-of-the-art methods, achieving superior performance in UGLAD. The code is available at <https://github.com/Yali-F/GLADMamba>.

Keywords: Unsupervised Graph-Level Anomaly Detection · Selective State Space Model · Graph Spectrum · Graph Neural Networks

1 Introduction

Unsupervised graph-level anomaly detection (UGLAD) is a prevalent task in numerous real-world scenarios, including social network analysis, drug discovery, and toxic molecule identification [16,20,21]. The goal is to identify graphs that

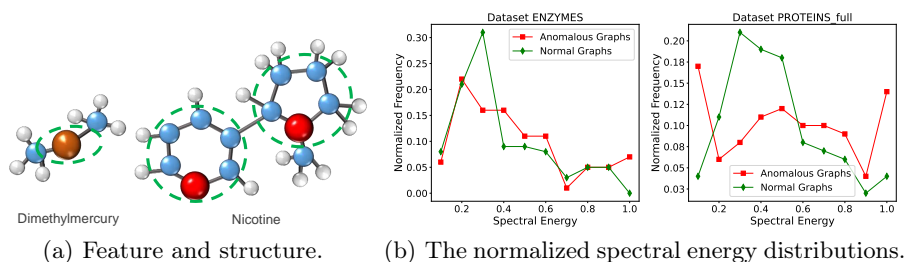


Fig. 1. The key factors related to UGLAD.

exhibit significantly different patterns from the majority, which often represent critical events or anomalies [18]. Unlike supervised approaches, unsupervised methods don’t require labeled data, making them more adaptable to real-world scenarios where labeled anomalies are scarce or costly to obtain. Despite the existence of many excellent methods, some challenges remain in this field.

Most GNN-based methods are inherently limited by the over-squashing issue, which restricts their ability to effectively model long-range dependencies between nodes [1,12,27]. This limitation hampers the propagation of information across distant nodes, making it challenging to capture anomaly-related patterns and ultimately weakening detection performance. Although some studies have incorporated Transformer into graph anomaly detection to mitigate this issue, the quadratic computational complexity of attention mechanism significantly restricts the scalability of these methods [16], particularly for large-scale graphs. Additionally, as depicted in Fig. 1(a), relying solely on a single aspect or characteristic is insufficient for comprehensively capturing anomalies [16,18]. Thus, effectively integrating multiple views (e.g., aspects or characteristics) presents a critical challenge.

Furthermore, we observe spectral differences between normal and abnormal graphs in Fig. 1(b). And as demonstrated in [4,31,33,38], the energy distribution in the spectral domain shifts from low-frequency to high-frequency regions as the anomaly degree increases. However, most existing methods primarily focus on anomaly information in the spatial domain, neglecting the interaction with the spectral domain and failing to account for the spectral differences between normal and anomalous graphs. Although a few works have explored the use of spectral information for graph-level anomaly detection, they rely on labeled data during training [4]. In the context of UGLAD, this remains an unexplored area, presenting a critical need for further research and innovation.

Recently, selective State Space Models (SSMs), especially Mamba [7], originally designed for sequence modeling, have demonstrated remarkable advantages in capturing long-range dependencies with linear computational complexity and selection mechanism. These advantages have been extensively validated across various domains [1,5,25,35,39], making Mamba a strong candidate for addressing the challenges in UGLAD. Building on these strengths, we take the first

step in integrating Mamba into UGLAD, unlocking its potential for more effective graph modeling while significantly improving computational efficiency and anomaly detection performance.

We propose a novel unsupervised graph-level anomaly detection framework that is powered by selective state space model (Mamba), dubbed as GLAD-Mamba. We firstly design the View-Fused Mamba (VFM), which is a Mamba-Transformer-style architecture and can efficiently fuse different views by Mamba’s selective state transition. Benefiting from its architecture and the advantages of Mamba, it excels at selecting key information related to anomaly detection and capturing long-range dependencies, showcasing its powerful embedding capabilities while maintaining linear time complexity. We also design Spectrum-Guided Mamba (SGM), which is another Mamba-Transformer-style architecture and can exploit explicit spectral information to guide the embedding refining process. It exploits the intrinsic relationship between spectral energy and anomalies on the graph scale, establishing interactions between the spatial and spectral domains. Concretely, it employs spectral energy to discretize the continuous state space, making the system parameters spectrum-dependent. Spectral energy guides the update of latent states in Mamba, enabling the model to selectively focus on anomaly-related information and filter redundant information.

By the selection mechanism, GLADMamba can dynamically adjust its learning strategy based on specific characteristics of different input graphs, adaptively capturing anomaly patterns. Extensive experiments on 12 real-world datasets demonstrate the effectiveness of GLADMamba. And the proposed GLADMamba consistently outperforms state-of-the-art methods in unsupervised graph-level anomaly detection. Our key contributions are summarized as follows:

- We propose a novel model, named GLADMamba, which adapts the Selective State Space Model (Mamba) for unsupervised graph-level anomaly detection. To the best of our knowledge, this is the first work to introduce Mamba to UGLAD.
- We design View-Fused Mamba (VFM) for efficient multi-view fusion, boosting detection accuracy. Also, we design Spectrum-Guided Mamba (SGM), the first spectrum-guided method to preserve anomaly-related patterns via selective state updates in this field. This work pioneers spectrum-guided Mamba architecture for UGLAD.
- We conduct extensive experiments on 12 real-world datasets, demonstrating that GLADMamba achieves state-of-the-art performance in unsupervised graph-level anomaly detection task.

2 Related Work

2.1 Graph-Level Anomaly Detection

Graph-level anomaly detection aims to identify anomalous graphs within a dataset, where anomalies typically represent rare but critical patterns compared to normal graphs [21]. Conventional methods generally involve two main steps: first,

a graph kernel, such as the Weisfeiler-Lehman kernel (WL) [28] or propagation kernel (PK) [24], is used to learn node representations. Second, an anomaly detection algorithm, such as isolation forest (iF) [17], one-class support vector machine (OCSVM) [22], or local outlier factor (LOF) [3], is applied to detect anomalous graphs based on the extracted graph representations.

In addition, graph neural networks (GNNs) have attracted significant attention due to their remarkable performance in dealing with graph data [11,14,32,34]. Thus, various types of GNN are employed as the backbone to conduct graph-level anomaly detection [6,16,18,19,20,40]. For example, GOOD-D [18] designs a novel graph data augmentation method and employs different level contrastive learning to conduct UGLAD. CVTGAD [16] employs a lightweight Transformer with an attention mechanism to model intra-graph and inter-graph node relationships, preserving key information.

2.2 State Space Models

State Space Models (SSMs) [13] are classical frameworks for dynamic systems, while Structured SSMs (S4) [10] enhance SSMs with efficient long-sequence modeling. Mamba [7,26] builds on S4 by introducing a selection mechanism, enabling dynamic adaptation and improved efficiency. Together, they represent an evolution from traditional SSMs to modern, high-performance sequence modeling architectures. Beyond its core advancements, Mamba has demonstrated promising applications in various domains. It has been explored in computer vision [35], multimodal learning [25], audio [5], and natural language processing [39], showcasing its versatility across different modalities. Mamba also has shown preliminary and promising applications in graph representation learning [1]. For example, DG-Mamba [37] introduces a kernelized dynamic message-passing operator and a self-supervised regularization based on the Principle of Relevant Information to improve efficiency, expressiveness, and robustness in dynamic graph learning. MOL-Mamba [12] enhances molecular representation by integrating hierarchical structural reasoning and electronic correlation learning through a hybrid Mamba-Graph and Mamba-Transformer framework, supported by collaborative training strategies.

3 Preliminaries

3.1 Problem Statement

A graph is represented as $G = (\mathcal{V}, \mathcal{E})$, where \mathcal{V} denotes the set of nodes and \mathcal{E} represents the set of edges. The entry $\mathbf{A}_{i,j}$ is set to 1 if an edge exists between node v_i and node v_j ; otherwise, $\mathbf{A}_{i,j} = 0$. An attributed graph is defined as $G = (\mathcal{V}, \mathcal{E}, \mathbf{X})$, where $\mathbf{X} \in \mathbb{R}^{n \times d_f}$ is the feature matrix containing node attributes. Each row of \mathbf{X} corresponds to a feature vector of a node with d_f dimensions. The collection of graphs is denoted as $\mathcal{G} = \{G_1, G_2, \dots, G_m\}$, where m is the total number of graphs. This work addresses the UGLAD problem, where no labels are available for model training.

3.2 State Space Models & Mamba

State Space Models (SSMs) [7,10,26] model the dynamic evolution of continuous system via latent state $h(t) \in \mathbb{R}^{N \times L}$, mapping input $x(t) \in \mathbb{R}^L$ to output $y(t) \in \mathbb{R}^L$ by state transition equation and observation equation, as follows:

$$h'(t) = \mathcal{A}h(t) + \mathcal{B}x(t), \quad y(t) = \mathcal{C}h(t), \quad (1)$$

where $\mathcal{A} \in \mathbb{R}^{N \times N}$ is the state transition matrix, $\mathcal{B} \in \mathbb{R}^{N \times 1}$ is the input matrix and $\mathcal{C} \in \mathbb{R}^{1 \times N}$ is the output matrix.

By the step size Δ , continuous parameters $(\mathcal{A}, \mathcal{B})$ are discretized into discrete parameters $(\bar{\mathcal{A}}, \bar{\mathcal{B}})$ for practical application of SSMs. Discrete SSMs are described as follows:

$$h_t = \bar{\mathcal{A}}h_{t-1} + \bar{\mathcal{B}}x_t, \quad y_t = \mathcal{C}h_t. \quad (2)$$

The selective SSMs (Mamba) [7] focuses on relevant information selectively by making parameters $(\mathcal{B}, \mathcal{C}, \Delta)$ input-dependent.

3.3 Rayleigh Quotient

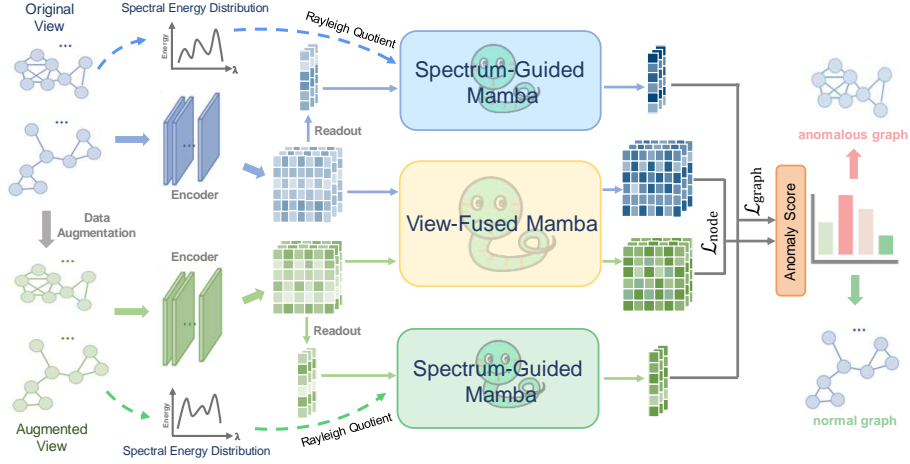
For a graph G , let \mathbf{A} be the adjacency matrix and \mathbf{D} be the diagonal degree matrix with $\mathbf{D}_{ii} = \sum_j \mathbf{A}_{ij}$. Its Laplacian matrix \mathbf{L} is defined as $\mathbf{L} = \mathbf{D} - \mathbf{A}$ (unnormalized) or $\mathbf{L} = \mathbf{I} - \mathbf{D}^{-1/2} \mathbf{A} \mathbf{D}^{-1/2}$ (normalized), where \mathbf{I} is the identity matrix. The symmetric matrix \mathbf{L} can be decomposed as $\mathbf{L} = \mathbf{U} \mathbf{\Lambda} \mathbf{U}^T$, where $\mathbf{\Lambda} = \text{diag}(\lambda_1, \lambda_2, \dots, \lambda_N)$ contains the corresponding eigenvalues sorted in ascending order, i.e., $0 \leq \lambda_1 \leq \lambda_2 \leq \dots \leq \lambda_N$, and $\mathbf{U} = (\mathbf{u}_1, \mathbf{u}_2, \dots, \mathbf{u}_N)$ represents the orthonormal eigenvectors. Let $\mathbf{X} = (x_1, x_2, \dots, x_N)^T$ be the signal of G , and its graph Fourier transform is given by $\hat{\mathbf{X}} = (\hat{x}_1, \hat{x}_2, \dots, \hat{x}_N) = \mathbf{U}^T \mathbf{X}$. As demonstrated in [4,31,33], the Rayleigh Quotient can represent the accumulated spectral energy, with higher value indicating more high-frequency component. We employ Rayleigh quotient without explicit eigenvalue decomposition for computational efficiency, as follows:

$$R(L, X) = \frac{X^T L X}{X^T X} = \frac{\sum_{k=1}^N \lambda_k \hat{x}_k^2}{\sum_{k=1}^N \hat{x}_k^2} = \frac{\sum_{(i,j) \in \mathcal{E}} (x_i - x_j)^2}{2 \sum_{i \in \nu} x_i^2}. \quad (3)$$

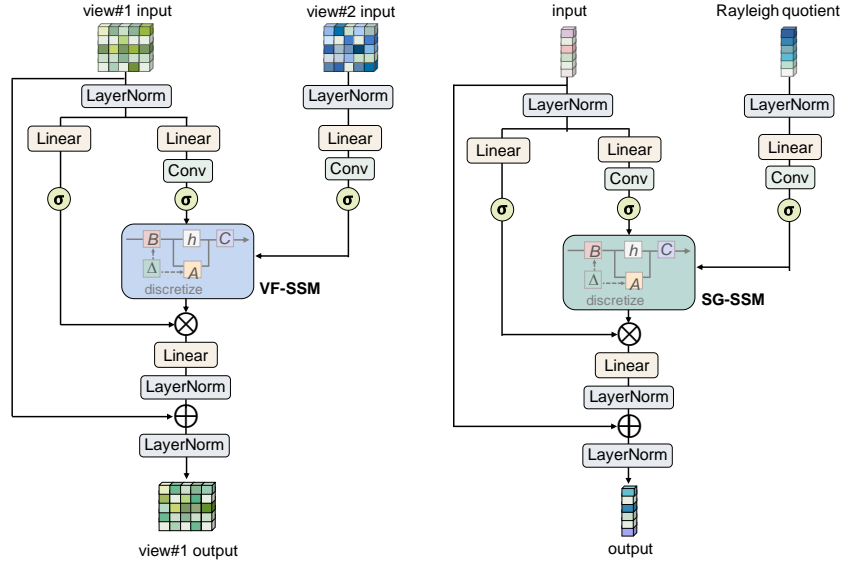
4 Methodology

4.1 Data Augmentation and Encoding

For the data augmentation, we obtain the original view o and augmented view a by perturbation-free graph augmentation strategy [16,18,30], which is tailored for anomaly detection. The view o and a consider feature and structure characteristics of the graph, respectively. After data augmentation, we employ two independent GNN encoders on two views to obtain node and graph embeddings.



(a) The overall pipeline of the proposed GLADMamba.



(b) View-Fused Mamba (VFM).

(c) Spectrum-Guided Mamba (SGM).

Fig. 2. Overview of the proposed GLADMamba model: (a) illustrates the overall pipeline of the framework; (b) depicts the View-Fused Mamba (VFM) module, which integrates multi-view information; (c) shows the Spectrum-Guided Mamba (SGM) module, which is designed to guide embedding refining process by Rayleigh quotient.

Taking the original view o as an example, GNN encoder updates node embeddings in the l -th layer according to following message passing rule:

$$\mathbf{h}_v^{(o,l)} = \text{UPDATE}^{(l-1)} \left(\mathbf{h}_v^{(o,l-1)}, \text{AGG}^{(l-1)} \left(\{ \mathbf{h}_u^{(o,l-1)} : u \in \mathcal{N}(v) \} \right) \right), \quad (4)$$

where $\mathbf{h}_v^{(o,l)}$ denotes the representation of node v on the view o at the l -th layer, $\mathcal{N}(v)$ represents the set of neighboring nodes of v , AGG is the aggregation function to combine information from neighboring nodes, and UPDATE is the update function to generate a new node representation. And we have $\mathbf{h}_v^{(o,0)} = \mathbf{x}_v$. After L -layer GNN encoder, we obtain the representation \mathbf{h}_v^o of node v by concatenation operation and the representation \mathbf{h}_G^o of graph G on the view o by the readout function:

$$\mathbf{h}_v^o = [\mathbf{h}_v^{(o,1)} || \dots || \mathbf{h}_v^{(o,L)}], \quad \mathbf{h}_G^o = \frac{1}{|\mathcal{V}_G|} \sum_{u \in \mathcal{V}_G} h_u^o, \quad (5)$$

where \mathcal{V}_G is the set of nodes in graph G . Let \mathbf{H}^o denote the node representations matrix encoded from the original view o in the training/testing batch, where each row corresponds to the representation of a node. In the same manner, we obtain the representation \mathbf{h}_v^a of node v , the representation \mathbf{h}_G^a of graph G , and the matrix \mathbf{H}^a on the view a .

4.2 View-Fused Mamba (VFM)

In the View-Fused Mamba (VFM) module, we propose an innovative view fusion mechanism. Specifically, we deeply fuse different aspects of graph data (feature and structure information) captured by the original view and augmented view. Designed in a Mamba-Transformer-style architecture, the VFM efficiently captures and processes multi-view information for UGLAD.

Selective Parameterization in VF-SSM. For the parameter \mathcal{A} , we adopt HiPPO-LegS [8] for parameterization [7,9]. Before obtaining the input-dependent parameters $(\mathcal{B}, \mathcal{C}, \Delta)$, we sequentially process the node representations \mathbf{H}^o and \mathbf{H}^a from two views through the following layers: a layer normalization [2], a linear projection layer, a 1D convolutional layer, and a SiLU activation function. The formulas are as follows:

$$\mathbf{H}_{input}^o = \text{SiLU}(\text{Conv1d}(\text{Linear}(\text{LayerNorm}(\mathbf{H}^o)))), \quad (6)$$

$$\mathbf{H}_{input}^a = \text{SiLU}(\text{Conv1d}(\text{Linear}(\text{LayerNorm}(\mathbf{H}^a)))). \quad (7)$$

When parameterizing input-dependent parameters \mathcal{B}, \mathcal{C} and Δ , the two views are fused through the following formulas:

$$\mathcal{B}^o = \mathbf{W}_{\mathcal{B}^o} \mathbf{H}_{input}^o, \quad \mathcal{C}^o = \mathbf{W}_{\mathcal{C}^o} \mathbf{H}_{input}^o, \quad \Delta^o = \text{softplus}(\mathbf{W}_{\Delta^o} \mathbf{H}_{input}^o), \quad (8)$$

$$\mathcal{B}^a = \mathbf{W}_{\mathcal{B}^a} \mathbf{H}_{input}^a, \quad \mathcal{C}^a = \mathbf{W}_{\mathcal{C}^a} \mathbf{H}_{input}^a, \quad \Delta^a = \text{softplus}(\mathbf{W}_{\Delta^a} \mathbf{H}_{input}^a), \quad (9)$$

where \mathbf{W} denotes the corresponding learnable matrix.

Selective Discretization in VF-SSM. To discretize the parameters \mathcal{A} and \mathcal{B} into $\bar{\mathcal{A}}$ and $\bar{\mathcal{B}}$, we adopt the zero-order hold (ZOH) discretization rule following [7,15].

$$\bar{\mathcal{A}}^o = \exp(\Delta^o \mathcal{A}^o), \quad \bar{\mathcal{B}}^o = (\Delta^o \mathcal{A}^o)^{-1} (\exp(\Delta^o \mathcal{A}^o) - I) (\Delta^o \mathcal{B}^o), \quad (10)$$

$$\bar{\mathcal{A}}^a = \exp(\Delta^a \mathcal{A}^a), \quad \bar{\mathcal{B}}^a = (\Delta^a \mathcal{A}^a)^{-1}(\exp(\Delta^a \mathcal{A}^a) - I)(\Delta^a \mathcal{B}^a). \quad (11)$$

After the discretization of system parameters, the VF-SSM in VFM performs $\text{SSM}(\bar{\mathcal{A}}^o, \bar{\mathcal{B}}^o, \mathbf{H}^o)$ and $\text{SSM}(\bar{\mathcal{A}}^a, \bar{\mathcal{B}}^a, \mathbf{H}^a)$ to update state selectively following Equation (2). The output of VF-SSM is as follows:

$$\begin{aligned} y_{ssm}^o &= \text{SSM}(\bar{\mathcal{A}}^o, \bar{\mathcal{B}}^o, \mathbf{H}_{input}^o), \\ y_{ssm}^a &= \text{SSM}(\bar{\mathcal{A}}^a, \bar{\mathcal{B}}^a, \mathbf{H}_{input}^a). \end{aligned} \quad (12)$$

After the View-Fused Mamba, we obtain the final output \mathbf{Z}^o and \mathbf{Z}^a as follows:

$$\begin{aligned} u^o &= \text{SiLU}(\text{Linear}(\text{LayerNorm}(\mathbf{H}^o))), \\ \mathbf{Z}^o &= \text{LayerNorm}(\text{LayerNorm}(\text{Linear}(y_{ssm}^o \odot u^o)) + \mathbf{H}^o), \\ u^a &= \text{SiLU}(\text{Linear}(\text{LayerNorm}(\mathbf{H}^a))), \\ \mathbf{Z}^a &= \text{LayerNorm}(\text{LayerNorm}(\text{Linear}(y_{ssm}^a \odot u^a)) + \mathbf{H}^a), \end{aligned} \quad (13)$$

where \odot denotes element-wise multiplication. The detailed architecture of the View-Fused Mamba is depicted in Fig. 2(b).

4.3 Spectrum-Guided Mamba (SGM)

We adopt the Rayleigh quotient as a measure of spectral characteristics which is closely related to anomalies, as described in Section 3.3. In the Spectrum-Guided Mamba (SGM) module, we introduce the Rayleigh quotient to guide the updates of the latent state. Designed in a Mamba-Transformer-style architecture, the SGM effectively refines embeddings by selectively focusing on anomaly-related information to enhance anomaly detection.

Selective Parameterization in SG-SSM. Let \mathbf{h}_G denote the graph representations encoded from the Section 4.1. Firstly, we utilize the MLP to obtain Rayleigh quotient representation, as follows:

$$\mathbf{h}_{RQ} = \text{MLP}(\text{diag}(R(L, X))), \quad (14)$$

where $\text{diag}(\cdot)$ extracts the diagonal elements of Rayleigh quotient $R(L, X)$.

The input \mathbf{h}_G and \mathbf{h}_{RQ} are passed through a series of layers, including layer normalization [2], a linear projection, a 1D convolutional operation, and a SiLU activation function, as follows:

$$\mathbf{h}_{input} = \text{SiLU}(\text{Conv1d}(\text{Linear}(\text{LayerNorm}(\mathbf{h}_G)))), \quad (15)$$

$$\mathbf{h}_{RQ} = \text{SiLU}(\text{Conv1d}(\text{Linear}(\text{LayerNorm}(\mathbf{h}_{RQ}))). \quad (16)$$

And we utilize obtained \mathbf{h}_{RQ} to parameterize \mathcal{B} , \mathcal{C} and Δ , as follows:

$$\mathcal{B} = \mathbf{W}_B \mathbf{h}_{RQ}, \quad \mathcal{C} = \mathbf{W}_C \mathbf{h}_{RQ}, \quad \Delta = \text{softplus}(\mathbf{W}_\Delta \mathbf{h}_{RQ}), \quad (17)$$

where \mathbf{W} is the corresponding learnable matrix. For the parameter \mathcal{A} , we still adopt HiPPO-LegS [8] for parameterization [7,9].

Selective Discretization in SG-SSM. According to the ZOH rule, we discretize the parameters \mathcal{A} and \mathcal{B} :

$$\bar{\mathcal{A}} = \exp(\Delta\mathcal{A}), \quad \bar{\mathcal{B}} = (\Delta\mathcal{A})^{-1}(\exp(\Delta\mathcal{A}) - I)(\Delta\mathcal{B}). \quad (18)$$

The SG-SSM in SGM performs $\text{SSM}(\bar{\mathcal{A}}, \bar{\mathcal{B}}, \mathbf{h}_{input})$ following Equation (2), yielding the output y_{ssm} :

$$y_{ssm} = \text{SSM}(\bar{\mathcal{A}}, \bar{\mathcal{B}}, \mathbf{h}_{input}). \quad (19)$$

After the Spectrum-Guided Mamba, we obtain the final output \mathbf{z}_G as follows:

$$\begin{aligned} u &= \text{SiLU}(\text{Linear}(\text{LayerNorm}(\mathbf{h}_G))), \\ \mathbf{z}_G &= \text{LayerNorm}(\text{LayerNorm}(\text{Linear}(y_{ssm} \odot u)) + \mathbf{h}_G). \end{aligned} \quad (20)$$

According to Equation (14)-(20), we obtain the graph representations \mathbf{z}_G^o and \mathbf{z}_G^a for the two views. And the detailed architecture of the Spectrum-Guided Mamba is depicted in Fig. 2(c).

4.4 Training and Inference

Training. We adopt the InfoNCE loss [41] as contrastive loss to maximize the agreement between the representations from two views on node and graph scales:

$$\begin{aligned} \mathcal{L}'_{node} &= \frac{1}{|B|} \sum_{G_j \in B} \frac{1}{2|V_{G_j}|} \sum_{v_i \in V_{G_j}} [\ell(\mathbf{z}_i^o, \mathbf{z}_i^a) + \ell(\mathbf{z}_i^a, \mathbf{z}_i^o)], \\ \ell(\mathbf{z}_i^o, \mathbf{z}_i^a) &= -\log \frac{e^{(\cos(\mathbf{z}_i^o, \mathbf{z}_i^a)/\tau)}}{\sum_{v_k \in V_{G_j} \setminus v_i} e^{(\cos(\mathbf{z}_i^o, \mathbf{z}_k^a)/\tau)}}, \end{aligned} \quad (21)$$

where B is the training batch, \mathbf{z}_i^o and \mathbf{z}_i^a are the embeddings of node v_i in two views, $\cos(\cdot)$ is the cosine similarity function, and τ is the temperature parameter.

$$\begin{aligned} \mathcal{L}'_{graph} &= \frac{1}{2|B|} \sum_{G_i \in B} [\ell(\mathbf{z}_{G_i}^o, \mathbf{z}_{G_i}^a) + \ell(\mathbf{z}_{G_i}^a, \mathbf{z}_{G_i}^o)], \\ \ell(\mathbf{z}_{G_i}^o, \mathbf{z}_{G_i}^a) &= -\log \frac{e^{\cos(\mathbf{z}_{G_i}^o, \mathbf{z}_{G_i}^a)/\tau}}{\sum_{G_j \in B \setminus G_i} e^{\cos(\mathbf{z}_{G_i}^o, \mathbf{z}_{G_j}^a)/\tau}}, \end{aligned} \quad (22)$$

where $\mathbf{z}_{G_i}^o$ and $\mathbf{z}_{G_i}^a$ are the embeddings of graph G_i in two views, and other notations are analogous to those in Equation (21).

During the training phase, we adopt adaptive loss \mathcal{L} to consider different sensitivities of node and graph scales for different datasets [16,18], as follows:

$$\begin{aligned} \mathcal{L}_{node} &= (\sigma_{node})^\alpha \mathcal{L}'_{node}, \quad \mathcal{L}_{graph} = (\sigma_{graph})^\alpha \mathcal{L}'_{graph}, \\ \mathcal{L} &= \mathcal{L}_{node} + \mathcal{L}_{graph}, \end{aligned} \quad (23)$$

where α is the hyper-parameter and σ is the standard deviation of predicted errors on the corresponding scale.

Inference. By minimizing \mathcal{L} in Equation (23) during the training, the model learns common patterns of normal graphs. When testing an anomalous graph, the \mathcal{L} tends to be significantly higher; therefore, we utilize the \mathcal{L} as the anomaly score. Additionally, the z-score standardization is adopted to balance anomaly scores from different scales. The anomaly score is formulated as:

$$S = \text{Std}(\mathcal{L}_{node}) + \text{Std}(\mathcal{L}_{graph}), \quad (24)$$

where $\text{Std}(\mathcal{L}) = (\mathcal{L} - \mu)/\sigma$, and μ is the mean values of predicted errors of training samples on the corresponding scale.

5 Experiments

5.1 Experiment Settings

Datasets. We conduct experiments on 12 public real-world datasets from Tu-Dataset benchmark [23], which involve small molecules, bioinformatics, and social networks. The statistics of the datasets are presented in Appendix A. Following the setting in [16,18], the samples in the minority class or real anomalous class are viewed as anomalies, while the rest are viewed as normal data. Similar to [16,18,20,40], only normal data are used for training.

Baselines. To evaluate the effectiveness of GLADMamba, we compare it with 9 competitive baselines, including both earlier and more recent approaches. These include the two-stage methods PK-iF [17,24], WL-OCSVM [22], WL-iF [28], InfoGraph+iF [29] and GraphCL+iF [36], and the end-to-end methods OCGIN [40], GLocalKD [20], GOOD-D [18] and CVTGAD [16]. Detailed descriptions of these baselines can be found in Appendix B.

Evaluation Metrics. Following [16,18,20], we use the area under the receiver operating characteristic curve (AUC) as the evaluation metric for UGLAD, where a higher AUC reflects better performance.

Implementation Details. We implement GLADMamba by PyTorch¹ on a NVIDIA L40 and a NVIDIA A40 GPU, and ensure reproducibility by explicitly setting random seeds following [16,18]. We employ GCN as the default GNN encoder. For AIDS, DHFR, HSE, and MMP datasets, the encoder employs GIN.

5.2 Overall Performance Comparison

We evaluate the performance of GLADMamba against several baselines in terms of AUC across 12 datasets. As summarized in Table 1, GLADMamba achieves the highest average rank, outperforming all baselines on 8 datasets and ranking second on the remaining 4. The results also show that unified models surpass two-stage methods, highlighting the advantages of end-to-end optimization for feature learning and anomaly detection. These findings underscore the effectiveness of GLADMamba in UGLAD across diverse domains.

¹ <https://pytorch.org/>

Table 1. Overall performance comparison in terms of AUC (%), mean±std). The best and second-best results are highlighted in **bold** and underlined, respectively.

Method	PK-iF†	WL-OCSVM†	WL-iF†	InfoGraph-iF†	GraphCL-iF†
ENZYMES	51.30±2.01	55.24±2.66	51.60±3.81	53.80±4.50	53.60±4.88
AIDS	51.84±2.87	50.12±3.43	61.13±0.71	70.19±5.03	79.72±3.98
DHFR	52.11±3.96	50.24±3.13	50.29±2.77	52.68±3.21	51.10±2.35
BZR	55.32±6.18	50.56±5.87	52.46±3.30	63.31±8.52	60.24±5.37
COX2	50.05±2.06	49.86±7.43	50.27±0.34	53.36±8.86	52.01±3.17
NCI1	50.58±1.38	50.63±1.22	50.74±1.70	50.10±0.87	49.88±0.53
IMDB-B	50.80±3.17	54.08±5.19	50.20±0.40	56.50±3.58	56.50±4.90
REDDIT-B	46.72±3.42	49.31±2.33	48.26±0.32	68.50±5.56	71.80±4.38
HSE	56.87±10.51	62.72±10.13	53.02±5.12	53.56±3.98	51.18±2.71
MMP	50.06±3.73	55.24±3.26	52.68±3.34	54.59±2.01	54.54±1.86
p53	50.69±2.02	54.59±4.46	50.85±2.16	52.66±1.95	53.29±2.32
PPAR-gamma	45.51±2.58	57.91±6.13	49.60±0.22	51.40±2.53	50.30±1.56
Avg.Rank	8.83	7.50	8.58	6.83	7.42
Method	OCGIN†	GLocalKD†	GOOD-D†	CVTGAD	GLADMamba
ENZYMES	58.75±5.98	61.39±8.81	63.90±3.69	<u>67.79±5.43</u>	68.39±4.55
AIDS	78.16±3.05	93.27±4.19	97.28±0.69	99.39±0.55	<u>99.29±0.47</u>
DHFR	49.23±3.05	56.71±3.57	62.67±3.11	<u>62.95±3.03</u>	63.79±4.16
BZR	65.91±1.47	69.42±7.78	75.16±5.15	<u>75.92±7.09</u>	77.25±4.62
COX2	53.58±5.05	59.37±12.67	62.65±8.14	<u>64.11±3.22</u>	66.38±1.40
NCI1	<u>71.98±1.21</u>	68.48±2.39	61.12±2.21	69.07±1.15	73.06±1.87
IMDB-B	60.19±8.90	52.09±3.41	65.88±0.75	70.97±1.35	<u>69.63±2.70</u>
REDDIT-B	75.93±8.65	77.85±2.62	88.67±1.24	84.97±2.41	<u>86.12±0.41</u>
HSE	64.84±4.70	59.48±1.44	69.65±2.14	<u>70.30±2.90</u>	71.19±2.68
MMP	<u>71.23±0.16</u>	67.84±0.59	70.57±1.56	70.96±1.01	73.19±3.22
p53	58.50±0.37	64.20±0.81	62.99±1.55	<u>67.58±3.31</u>	68.38±1.62
PPAR-gamma	71.19±4.28	64.59±0.67	67.34±1.71	68.25±4.66	<u>69.21±3.46</u>
Avg.Rank	4.50	4.58	3.25	<u>2.17</u>	1.33

5.3 Ablation Study

To validate the effectiveness of different components of GLADMamba, we conduct extensive ablation experiments on 8 representative datasets in Fig. 3. The variant *w/o* VF-SSM represents modifying the selective parameterization and discretization processes by the inputs under the corresponding view in the VF-SSM. The variant *w/o* SG-SSM replaces the Rayleigh quotient in the SG-SSM with the corresponding graph-level representations. The variants *w/o* VFM, *w/o* SGM, and *w/o* Mamba denote the removal of the View-Fused Mamba, the Spectrum-Guided Mamba, and both, respectively.

The results demonstrate that GLADMamba consistently outperforms all variants. The variant *w/o* VFM, *w/o* SGM, and *w/o* Mamba significantly degrade performance, validating the effectiveness of the Mamba in UGLAD task

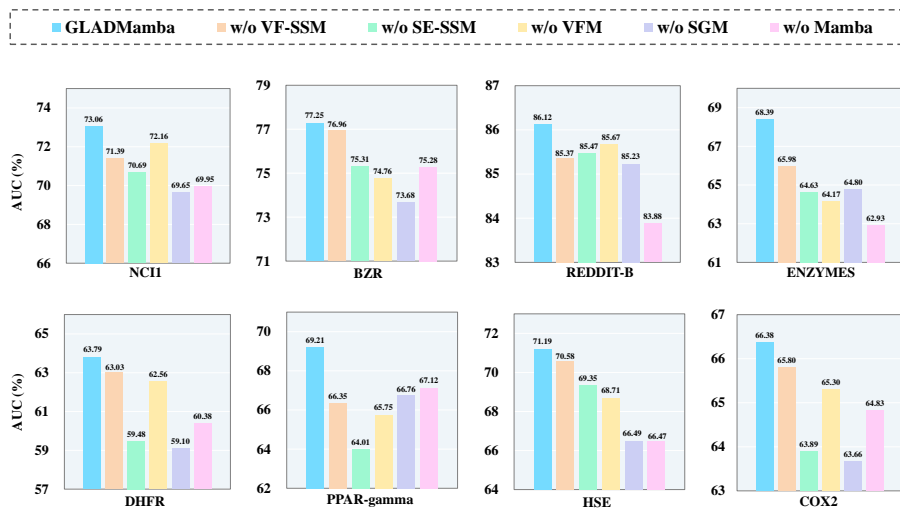


Fig. 3. Ablation study on key components on representative datasets.

and its superiority in capturing long-range dependencies and key anomaly patterns in graphs. And *w/o* VF-SSM which relies solely on single-view information, suffers a performance decline, limiting GLADMamba’s ability to identify complex anomalies. Furthermore, the significant performance drop in the *w/o* SG-SSM demonstrates the importance of spectral differences between normal and anomalous graphs for guiding the latent state updates of GLADMamba. The SG-SSM further enhances GLADMamba’s sensitivity to anomaly-related information.

5.4 Efficiency Analysis

We assess the efficiency of GLADMamba on representative datasets in terms of FLOPs, parameter size, and GPU usage in Table 2. On the small-scale molecular dataset AIDS, the complexity differences between CVTGAD and GLADMamba are tolerable. However, on larger-scale datasets REDDIT-B and p53, the complexity differences become significant, particularly in terms of FLOPs and parameter size. This demonstrates the superiority of GLADMamba over Transformer-based approaches in scaling to large-scale graph anomaly detection.

5.5 Hyper-Parameter Analysis

The state size of VFM and SGM. To investigate the impact of state size, we conduct analysis experiments in Fig. 4(a). The results indicate that performance variations with state size are not entirely consistent across datasets, likely due to the dependency of state size on the dataset scale. Overall, the model can achieve satisfactory performance at smaller values (e.g., 4, 8).

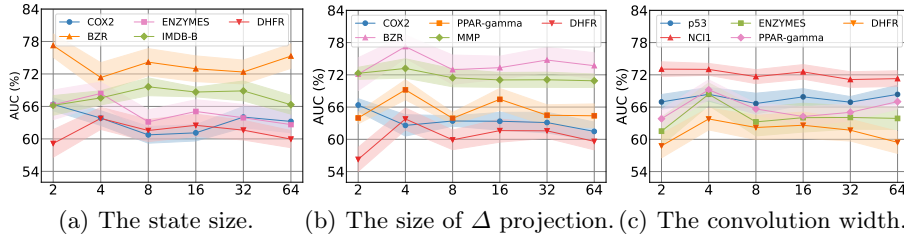


Fig. 4. The hyper-parameter analysis on representative datasets.

The size of Δ projection of VFM and SGM. The parameter Δ is constructed by the linear projection of the input, controlling the strength of state updates. To investigate the impact of Δ projection size, we conduct experiments in Fig. 4(b). The results demonstrate that the model generally performs worst when the size is 2, except for COX2 dataset. In general, the model can achieve respectable performance when the size is 4. As the projection size increases further, the performance is relatively stable overall. These findings indicate that a moderate size (e.g., 4) is sufficient for optimal performance, avoiding suboptimal performance or unnecessary resource overhead.

The local convolution width of VFM and SGM. The local convolution width is the kernel size of the Conv1D layer, controlling the receptive field of the model. We conduct experiments to investigate its impact in Fig. 4(c). We observe that when the width is 2, the performance degrades due to limited expressiveness of the Conv1D. In most cases, the model achieves optimal performance when the width is 4. Overall, GLADMamba remains relatively insensitive to this parameter, demonstrating robust performance.

5.6 Visualization Analysis

We utilize t-SNE to visualize the graph embeddings from two views and anomaly scores learned by GLADMamba in Fig. 5. It can be observed that normal and anomalous graphs are not well-separated under a single view, as the distribution

Table 2. Efficiency comparison on FLOPs, parameter size, and GPU memory usage.

Dataset	Model	FLOPs (M)↓	Params (MB)↓	GPU (GB)↓
AIDS	CVTGAD	33.27	1.88	8.58
	GLADMamba	48.97	0.07	5.12
REDDIT-B	CVTGAD	602.46	13.19	30.70
	GLADMamba	431.59	0.11	23.79
p53	CVTGAD	701.31	20.61	4.98
	GLADMamba	226.19	0.08	3.96

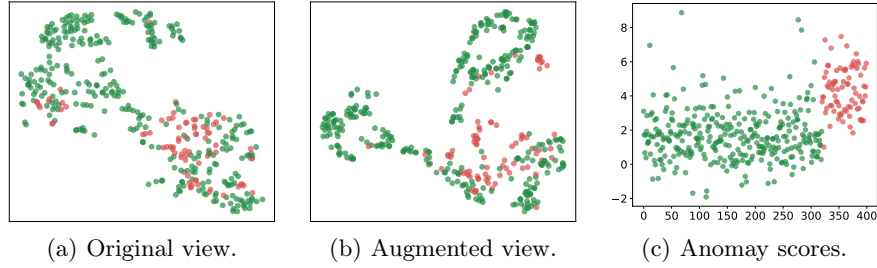


Fig. 5. Visualization analysis on AIDS dataset. (● normal graph, ● anomalous graph.)

exhibits considerable overlap. However, when multiple views are integrated, normal and anomalous graphs exhibit a clear boundary in anomaly scores, demonstrating the effectiveness of GLADMamba in UGLAD.

6 Conclusion

In this work, we introduce GLADMamba, a novel framework for UGLAD that effectively integrates the selective state space model and explicit spectral information. By leveraging the View-Fused Mamba and Spectrum-Guided Mamba, GLADMamba dynamically selects and refines anomaly-related information, significantly improving detection performance. As far as we know, this is the first work to introduce Mamba and explicit spectral information to UGLAD. Experimental results on multiple real-world datasets demonstrate that GLADMamba outperforms existing state-of-the-art methods, highlighting its potential for advancing the UGLAD field. This fundamental architecture advancement establishes new possibilities for both graph learning and anomaly detection research.

References

1. Atitallah, S.B., Rabah, C.B., Driss, M., Boulila, W., Koubaa, A.: Exploring graph mamba: A comprehensive survey on state-space models for graph learning. arXiv preprint arXiv:2412.18322 (2024)
2. Ba, J.L., Kiros, J.R., Hinton, G.E.: Layer normalization. arXiv preprint arXiv:1607.06450 (2016)
3. Breunig, M.M., Kriegel, H.P., Ng, R.T., Sander, J.: Lof: identifying density-based local outliers. In: Proceedings of the 2000 ACM SIGMOD international conference on Management of data. pp. 93–104 (2000)
4. Dong, X., Zhang, X., Wang, S.: Rayleigh quotient graph neural networks for graph-level anomaly detection. arXiv preprint arXiv:2310.02861 (2023)
5. Erol, M.H., Senocak, A., Feng, J., Chung, J.S.: Audio mamba: Bidirectional state space model for audio representation learning. IEEE Signal Processing Letters (2024)

6. Fu, Y., Li, J., Liu, J., Xing, Q., Wang, Q., King, I.: Hc-glad: Dual hyperbolic contrastive learning for unsupervised graph-level anomaly detection. arXiv preprint arXiv:2407.02057 (2024)
7. Gu, A., Dao, T.: Mamba: Linear-time sequence modeling with selective state spaces. arXiv preprint arXiv:2312.00752 (2023)
8. Gu, A., Dao, T., Ermon, S., Rudra, A., Ré, C.: Hippo: Recurrent memory with optimal polynomial projections. *Advances in neural information processing systems* **33**, 1474–1487 (2020)
9. Gu, A., Goel, K., Gupta, A., Ré, C.: On the parameterization and initialization of diagonal state space models. *Advances in Neural Information Processing Systems* **35**, 35971–35983 (2022)
10. Gu, A., Goel, K., Re, C.: Efficiently modeling long sequences with structured state spaces. In: *International Conference on Learning Representations* (2022)
11. Hamilton, W., Ying, Z., Leskovec, J.: Inductive representation learning on large graphs. *Advances in neural information processing systems* **30** (2017)
12. Hu, J., Guo, D., Si, Z., Liu, D., Diao, Y., Zhang, J., Zhou, J., Wang, M.: Molmamba: Enhancing molecular representation with structural & electronic insights. arXiv preprint arXiv:2412.16483 (2024)
13. Kalman, R.E.: A new approach to linear filtering and prediction problems (1960)
14. Kipf, T.N., Welling, M.: Semi-supervised classification with graph convolutional networks. arXiv preprint arXiv:1609.02907 (2016)
15. Li, D., Tan, S., Zhang, Y., Jin, M., Pan, S., Okumura, M., Jiang, R.: Dymamba: Continuous state space modeling on dynamic graphs. arXiv preprint arXiv:2408.06966 (2024)
16. Li, J., Xing, Q., Wang, Q., Chang, Y.: Cvtgad: simplified transformer with cross-view attention for unsupervised graph-level anomaly detection. In: *Joint European Conference on Machine Learning and Knowledge Discovery in Databases*. pp. 185–200. Springer (2023)
17. Liu, F.T., Ting, K.M., Zhou, Z.H.: Isolation forest. In: *2008 eighth IEEE international conference on data mining*. pp. 413–422. IEEE (2008)
18. Liu, Y., Ding, K., Liu, H., Pan, S.: Good-d: On unsupervised graph out-of-distribution detection. In: *Proceedings of the Sixteenth ACM International Conference on Web Search and Data Mining*. pp. 339–347 (2023)
19. Luo, X., Wu, J., Yang, J., Xue, S., Peng, H., Zhou, C., Chen, H., Li, Z., Sheng, Q.Z.: Deep graph level anomaly detection with contrastive learning. *Scientific Reports* **12**(1), 19867 (2022)
20. Ma, R., Pang, G., Chen, L., van den Hengel, A.: Deep graph-level anomaly detection by glocal knowledge distillation. In: *Proceedings of the fifteenth ACM international conference on web search and data mining*. pp. 704–714 (2022)
21. Ma, X., Wu, J., Xue, S., Yang, J., Zhou, C., Sheng, Q.Z., Xiong, H., Akoglu, L.: A comprehensive survey on graph anomaly detection with deep learning. *IEEE transactions on knowledge and data engineering* **35**(12), 12012–12038 (2021)
22. Manevitz, L.M., Yousef, M.: One-class svms for document classification. *Journal of machine Learning research* **2**(Dec), 139–154 (2001)
23. Morris, C., Kriege, N.M., Bause, F., Kersting, K., Mutzel, P., Neumann, M.: Tudataset: A collection of benchmark datasets for learning with graphs. arXiv preprint arXiv:2007.08663 (2020)
24. Neumann, M., Garnett, R., Bauckhage, C., Kersting, K.: Propagation kernels: efficient graph kernels from propagated information. *Machine learning* **102**, 209–245 (2016)

25. Qiao, Y., Yu, Z., Guo, L., Chen, S., Zhao, Z., Sun, M., Wu, Q., Liu, J.: Vl-mamba: Exploring state space models for multimodal learning. arXiv preprint arXiv:2403.13600 (2024)
26. Qu, H., Ning, L., An, R., Fan, W., Derr, T., Liu, H., Xu, X., Li, Q.: A survey of mamba. arXiv preprint arXiv:2408.01129 (2024)
27. Qureshi, S., et al.: Limits of depth: Over-smoothing and over-squashing in gnns. *Big Data Mining and Analytics* **7**(1), 205–216 (2023)
28. Shervashidze, N., Schweitzer, P., Van Leeuwen, E.J., Mehlhorn, K., Borgwardt, K.M.: Weisfeiler-lehman graph kernels. *Journal of Machine Learning Research* **12**(9) (2011)
29. Sun, F.Y., Hoffman, J., Verma, V., Tang, J.: Infograph: Unsupervised and semi-supervised graph-level representation learning via mutual information maximization. In: *International Conference on Learning Representations* (2020)
30. Tan, Y., Liu, Y., Long, G., Jiang, J., Lu, Q., Zhang, C.: Federated learning on non-iid graphs via structural knowledge sharing. In: *Proceedings of the AAAI conference on artificial intelligence*. vol. 37, pp. 9953–9961 (2023)
31. Tang, J., Li, J., Gao, Z., Li, J.: Rethinking graph neural networks for anomaly detection. In: *International conference on machine learning*. pp. 21076–21089. PMLR (2022)
32. Veličković, P., Cucurull, G., Casanova, A., Romero, A., Lio, P., Bengio, Y.: Graph attention networks. arXiv preprint arXiv:1710.10903 (2017)
33. Xu, F., Wang, N., Wu, H., Wen, X., Zhao, X., Wan, H.: Revisiting graph-based fraud detection in sight of heterophily and spectrum. In: *Proceedings of the AAAI conference on artificial intelligence*. vol. 38, pp. 9214–9222 (2024)
34. Xu, K., Hu, W., Leskovec, J., Jegelka, S.: How powerful are graph neural networks? arXiv preprint arXiv:1810.00826 (2018)
35. Xu, R., Yang, S., Wang, Y., Du, B., Chen, H.: A survey on vision mamba: Models, applications and challenges. arXiv e-prints pp. arXiv-2404 (2024)
36. You, Y., Chen, T., Sui, Y., Chen, T., Wang, Z., Shen, Y.: Graph contrastive learning with augmentations. *Advances in neural information processing systems* **33**, 5812–5823 (2020)
37. Yuan, H., Sun, Q., Wang, Z., Fu, X., Ji, C., Wang, Y., Jin, B., Li, J.: Dg-mamba: Robust and efficient dynamic graph structure learning with selective state space models. arXiv preprint arXiv:2412.08160 (2024)
38. Zang, Y., Ren, L., Li, Y., Wang, Z., Selby, D.A., Wang, Z., Vollmer, S.J., Yin, H., Song, J., Wu, J.: Rethinking cancer gene identification through graph anomaly analysis. arXiv preprint arXiv:2412.17240 (2024)
39. Zhao, H., Zhang, M., Zhao, W., Ding, P., Huang, S., Wang, D.: Cobra: Extending mamba to multi-modal large language model for efficient inference. arXiv preprint arXiv:2403.14520 (2024)
40. Zhao, L., Akoglu, L.: On using classification datasets to evaluate graph outlier detection: Peculiar observations and new insights. *Big Data* **11**(3), 151–180 (2023)
41. Zhu, Y., Xu, Y., Yu, F., Liu, Q., Wu, S., Wang, L.: Graph contrastive learning with adaptive augmentation. In: *Proceedings of the web conference 2021*. pp. 2069–2080 (2021)

A Dataset Details

Table 3 summarizes the statistics of the 12 public real-world datasets used in our experiments. Each dataset corresponds to one row in the table, and four key attributes are reported:

- **Graphs:** The total number of graphs in the dataset.
- **Average Nodes:** The average number of nodes per graph.
- **Average Edges:** The average number of edges per graph.
- **Attributes:** The dimensionality of node attributes. A numerical value indicates the attribute dimension, while ‘-’ denotes that the dataset consists of attribute-free graphs (i.e., nodes have no attributes).

These datasets span various domains, including small molecules, bioinformatics, and social networks. They provide diverse structures and characteristics, ensuring a comprehensive evaluation of graph-level anomaly detection methods.

Table 3. Statistics of the datasets [23] used in our experiments.

Dataset	Graphs	Avg. Nodes	Avg. Edges	Attributes
ENZYMES	600	32.63	62.14	18
AIDS	2000	15.69	16.20	4
DHFR	467	42.43	44.54	3
BZR	405	35.75	38.36	3
COX2	467	41.22	43.45	3
NCI1	4110	29.87	32.30	-
IMDB-B	1000	19.77	96.53	-
REDDIT-B	2000	429.63	497.75	-
HSE	8417	16.89	17.23	-
MMP	7558	17.62	17.98	-
p53	8903	17.92	18.34	-
PPAR-gamma	8451	17.38	17.72	-

B Baseline Details

We provide additional details about the baselines used for performance comparison with GLADMamba.

The baselines used in our experiments include two-stage methods: PK-iF, WL-OCSVM, WL-iF, InfoGraph+iF and GraphCL+iF. These methods first generate graph embeddings using graph kernels (e.g., propagation kernel or Weisfeiler-Lehman kernel) or graph representation learning methods, and then apply traditional anomaly detection algorithms (e.g., isolation forest or one-class SVM) to identify anomalies.

- **PK-iF**: A method leveraging the propagation kernel [24] for graph embedding, combined with isolation forest [17] for anomaly detection. The propagation kernel learns graph-level embeddings, while isolation forest identifies anomalies based on their isolation characteristics in the embedding space.
- **WL-OCSVM**: A method using the Weisfeiler-Lehman kernel [28] for graph embedding, and the one-class SVM [22] to learn a decision boundary for anomaly detection.
- **WL-iF**: A method combining the Weisfeiler-Lehman kernel for graph embedding and isolation forest [17] for anomaly detection.
- **InfoGraph+iF**: A method combining InfoGraph [29], a graph representation learning framework based on mutual information maximization, with isolation forest for anomaly detection.
- **GraphCL+iF**: A method combining GraphCL [36], learning graph embeddings by contrastive learning, with isolation forest for anomaly detection.

Additionally, we compare against end-to-end methods: OCGIN, GLocalKD, GOOD-D, and CVTGAD. These approaches integrate graph representation learning and anomaly detection into a unified framework, enabling joint optimization.

- **OCGIN [40]**: OCGIN is a graph-level graph anomaly detection model based on the Graph Isomorphism Network (GIN), which is adapted from graph classification tasks. Unlike traditional two-stage methods, OCGIN is trained end-to-end using a one-class classification objective.
- **GLocalKD [20]**: GLocalKD introduces a joint random distillation mechanism that learns global and local normal patterns by training one graph neural network (GNN) to predict the representations of another GNN with randomly initialized weights.
- **GOOD-D [18]**: GOOD-D is a framework designed for graph-level graph anomaly detection, leveraging hierarchical contrastive learning to capture normal patterns at multiple granularities, including node-level, graph-level, and group-level representations. Anomalies are detected based on their semantic inconsistency with the learned patterns.
- **CVTGAD [16]**: CVTGAD is designed for unsupervised graph-level graph anomaly detection by introducing a simplified Transformer to capture relationships between intra-graph and inter-graph perspectives.